

Supplementary Information

Orientational structures in cholesteric droplets with homeotropic surface anchoring

Mikhail N. Krakhalev,^{1,2} Vladimir Yu. Rudyak,^{3,*} Oxana O. Prishchepa,^{1,2} Anna P. Gardymova,² Alexander V. Emelyanenko,³ Jui-Hsiang Liu,⁴ and Victor Ya. Zyryanov¹

¹*Kirensky Institute of Physics, Federal Research Center KSC SB RAS, Krasnoyarsk 660036, Russia*

²*Institute of Engineering Physics and Radio Electronics,
Siberian Federal University, Krasnoyarsk 660041, Russia*

³*Faculty of Physics, Lomonosov Moscow State University, Moscow, 119991 Russia*

⁴*Department of Chemical Engineering, National Cheng Kung University, Tainan 70101, Taiwan*

(Dated: June 4, 2019)

* vurdizm@gmail.com

Test of discretization problem of the simulations technique

The simulations technique used in this work utilizes cubic lattice for space discretization. We tested the affect of cubic lattice on discretization of the positions and energies of the disclination lines in our simulations.

For this, we analyzed two transitions: twisted radial to toron-like (**tR**-**T**) and intermediate to layer-like (**L**₀-**L**). For both cases, we selected the pair of concurring structures near the phase transition point (**tR** at $N_0 = 3.12$, **T** at $N_0 = 3.25$, **L**₀ at $N_0 = 6.02$ and **L** at $N_0 = 6.15$).

For each of these structures, we generated 10 random rotations in all three degrees of freedom. For this, each structure was rotated in sequence: around Oz by ψ , around Oy by θ , and then around Oz by ϕ . Ten values of angles $\psi \in [0, 2\pi]$, $\theta \in [0, \pi]$ and $\phi \in [0, 2\pi]$ were randomly generated for each of four initial structures.

Then we produced local optimization of these structures in the small region of N_0 around the transition point ($3.0 \leq N_0 \leq 3.38$ for **tR** and **T**, $5.63 \leq N_0 \leq 6.0$ for **L**₀ and **L**).

First, we analyzed the optimized structures. All structures were of the same type as the corresponding structures before rotation and reproduced it with minor deviations. Sample structures shown below are randomly chosen from the pool:

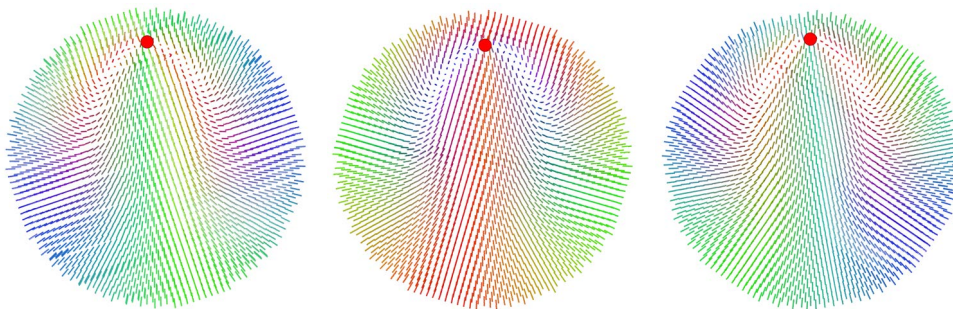


Figure 1. Twisted radial (**tR**) structures locally optimized after random rotation.

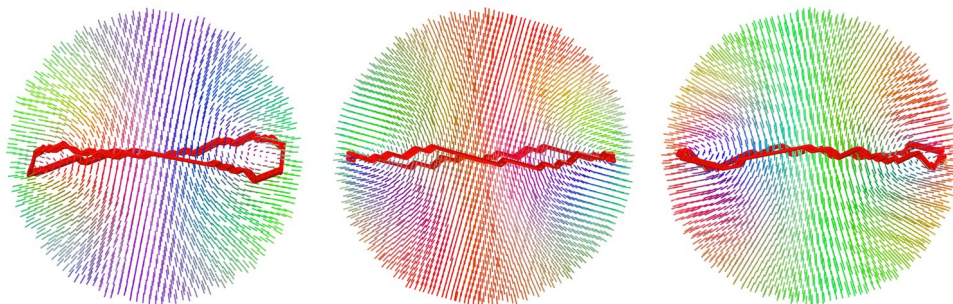


Figure 2. Toron-like (**T**) structures locally optimized after random rotation.

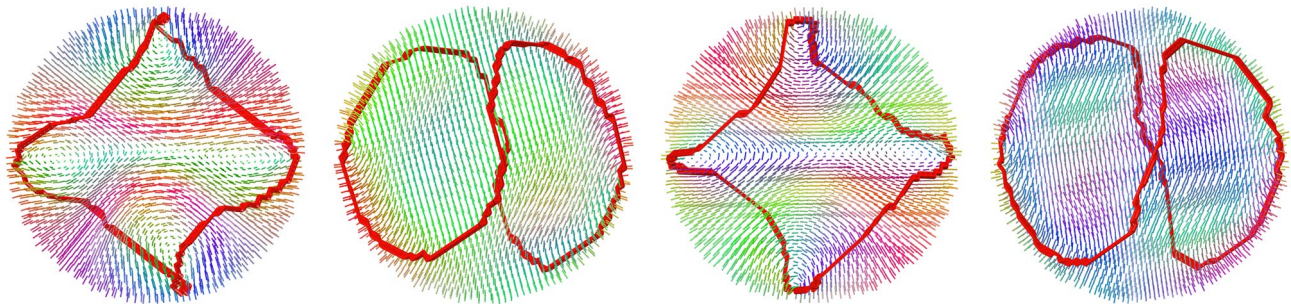


Figure 3. Intermediate (\mathbf{L}_0) structures locally optimized after random rotation (in pairs, each pair contains cross-cut in orthogonal planes).

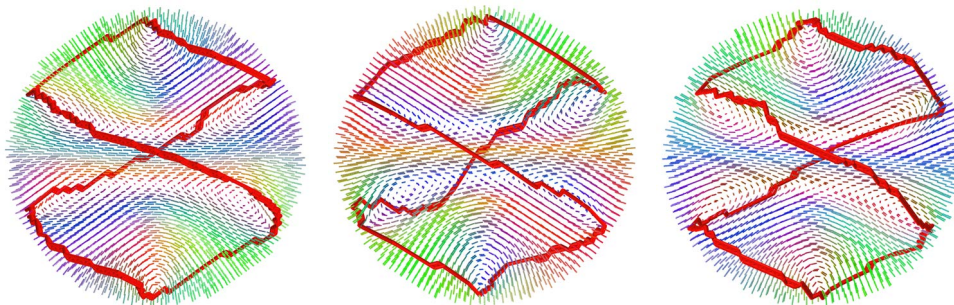


Figure 4. Layer-like (\mathbf{L}) structures locally optimized after random rotation.

Second, we calculated average free energies and standard deviations for each structure type for each value of N_0 (i.e. data for 10 independent locally optimized structures were averaged for each point). It can be seen, that the errors are relatively small, and in both cases transitions remain at approximately the same values of N_0 (dash lines show the positions of transitions from Fig. 6).

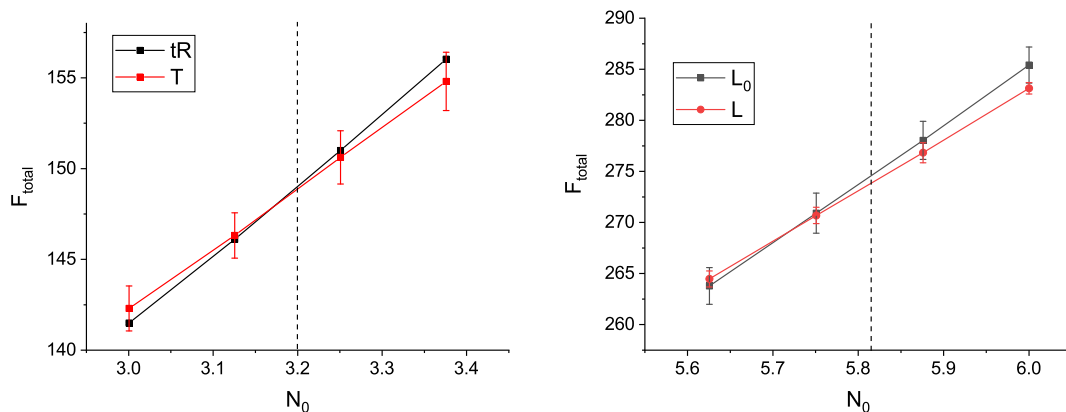


Figure 5. Average total free energy and its standard deviation for various structure types near \mathbf{tR} - \mathbf{T} (left) and \mathbf{L}_0 - \mathbf{L} phase transitions.

Finally, we plotted standard deviations per energy term for \mathbf{tR} and \mathbf{T} structures (averaged by four values of N_0) to investigate the effect of rotation in more details. The deviation of the defect energy is relatively small, compared to the scale of energy changes in this system. Moreover, when the defect is located close to the surface, the highest deviation comes from surface energy, which is also small enough to make confident conclusions about structural changes in this system.

These data clearly shows that the positions of disclination lines are only slightly aligned by the cubic lattice. In overall the discretization effect is minor for both defect position and energy in the simulations method used in this work.

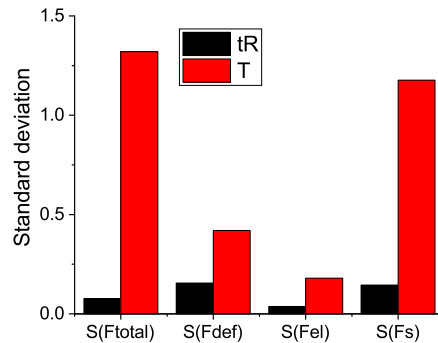


Figure 6. Standard deviations of total free energy and its terms in **tR** and **T** structures (averaged for $3.0 \leq N_0 \leq 3.38$).

L_0 - L transition

To investigate the origin of stability of two layer-like states, we calculated the dependencies of total free energy of layer-like states with different defect length for each N_0 in the region between 5.2 and 6.0. For each value of N_0 , two energy minima were identified: one with low director twist (layer-like intermediate structure, L_0) and one with normal director twist (layer-like structure, L). The states between L_0 and L were found to be energetically less favorable, effectively forming energy barrier preventing gradual twist of L_0 structure to L structure at high N_0 s. At $N_0 \approx 5.8$ the regular L structure becomes more favorable, which leads to the first order phase transition in the system (with corresponding hysteresis in experimental setup). Figures 7 and 8 below show the total and detailed energy balance leading to this situation. Notably, the estimation of the free energy balance for the material with $K_{11} = K_{22} = K_{33}$ leads to the only L structure energetically favorable on the whole range of N_0 . We made this estimation by renormalization F_{splay} , F_{twist} , and F_{bend} . It can be concluded that the different material properties will lead to different phase diagrams in this region of N_0 , with or without presence of intermediate layer-like structure L_0 .

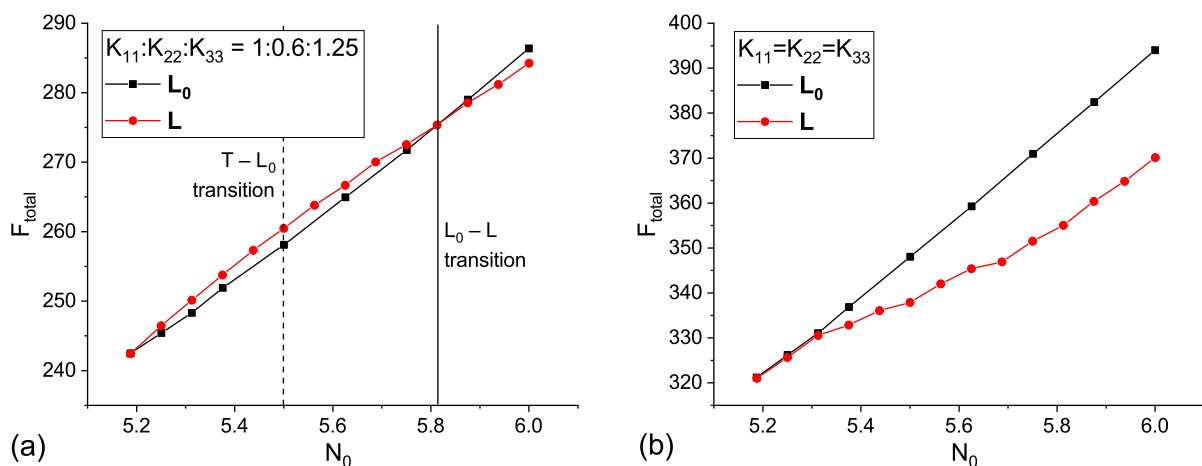


Figure 7. Dependencies of the total free energy of L_0 and L states on N_0 for (a) E7 : Ch = 97 : 3 and (b) single constant approximation (estimation).

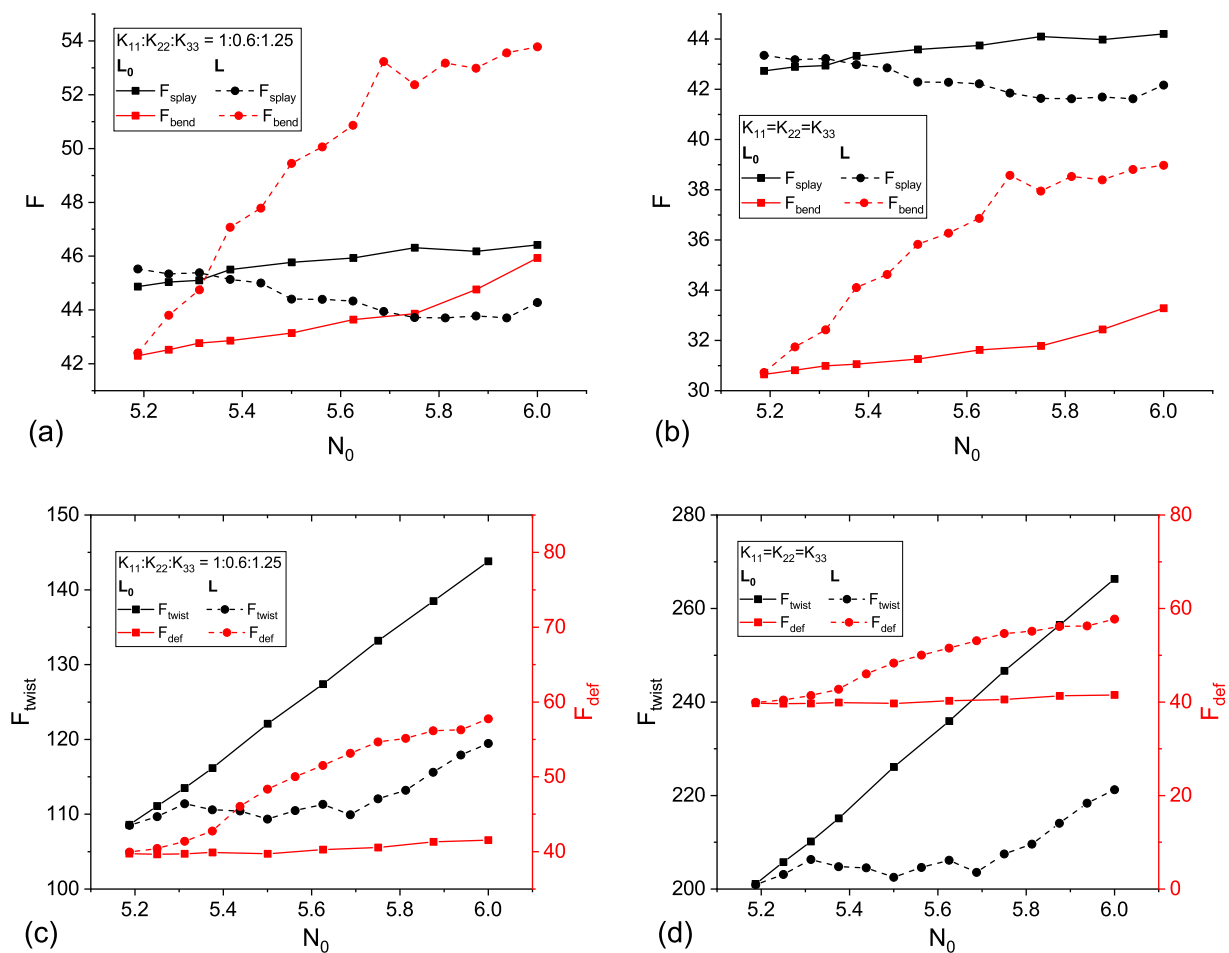


Figure 8. Dependencies of various free energy terms of L_0 and L states on N_0 for (a, c) E7 : Ch = 97 : 3 and (b, d) single constant approximation (estimation).

Additional experimental data

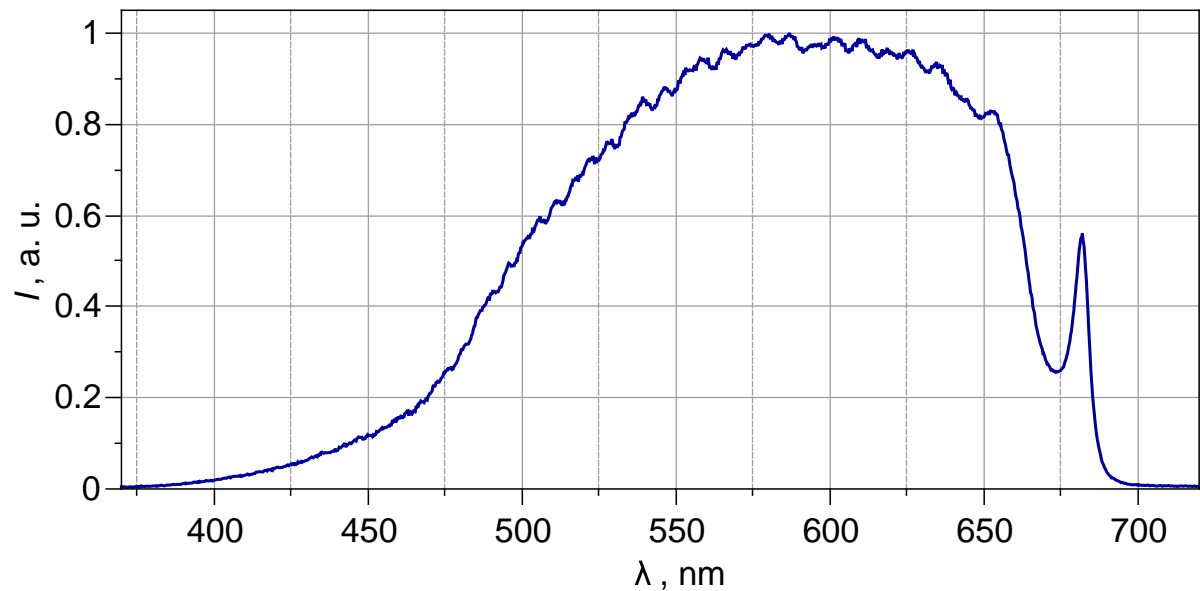


Figure 9. The spectrum of the microscope halogen lamp taken after light propagation through the condenser, the polarizer, and the objective. The measurement was made by the HR4000CG-UV-NIR spectrometer (Ocean Optics).

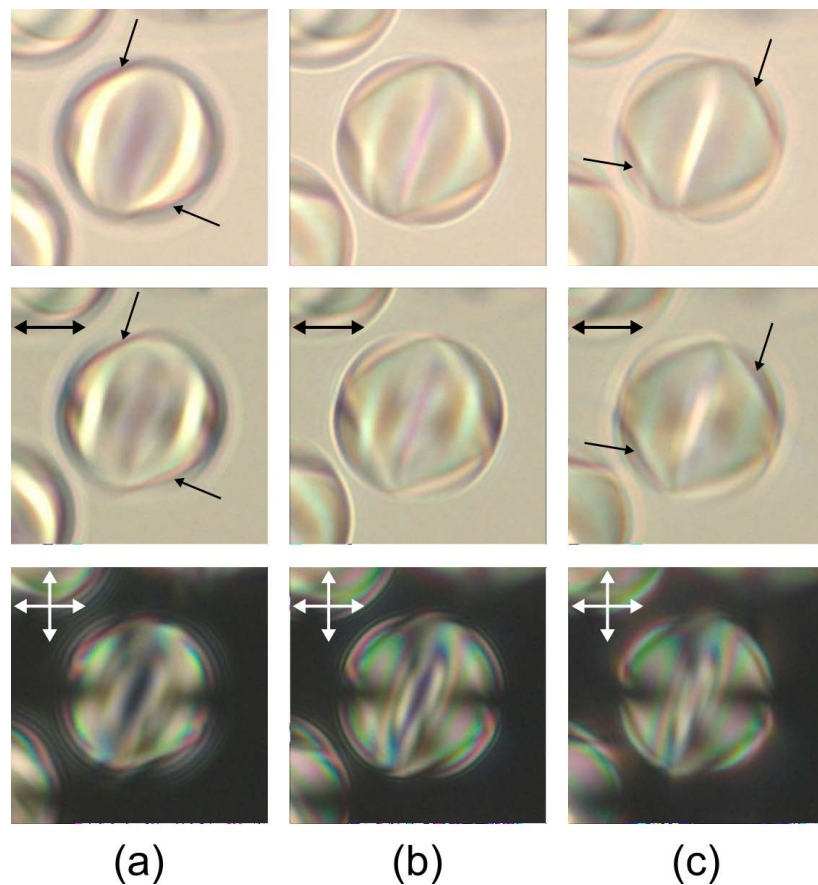


Figure 10. Photos of the droplet with the intermediate (L_0) structure shown in Fig. 4 (top row) taken in the unpolarized light (top row), at switched-off analyzer (middle row) and in the crossed polarizers (bottom row). The microscope is focused on the curved defect loop above (a), on (b) and below (c) of the central cross-section of the droplet. Hereinafter, the polarizer's directions are indicated by the double arrows, the single arrows indicate at the linear defect.

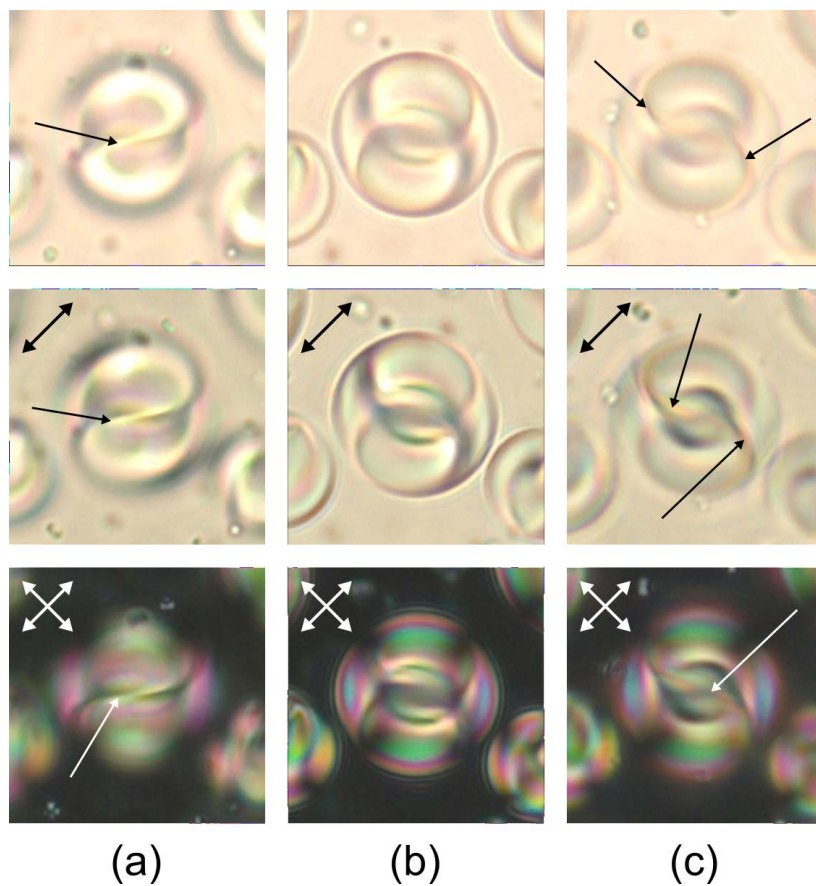


Figure 11. Photos of the droplet with the intermediate (L_0) structure shown in Fig. 4 (bottom row) taken in the unpolarized light (top row), at switched-off analyzer (middle row) and in the crossed polarizers (bottom row). The microscope is focused on the curved defect loop above (a), on (b) and below (c) of the central cross-section of the droplet.

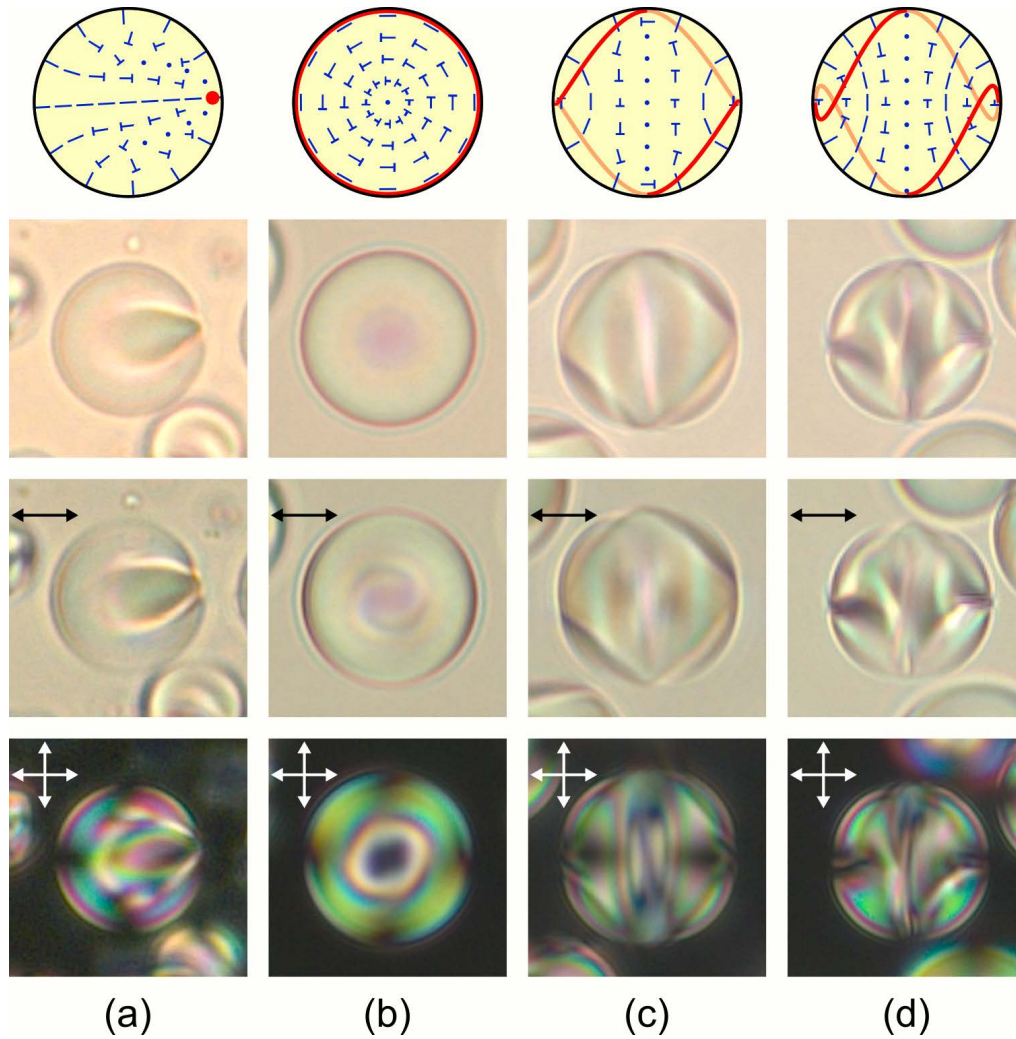


Figure 12. Four structures observed in droplets with $4.7 \leq N_0 \leq 5.5$: twisted radial (**tR**) (a), toron-like (**T**) (b), intermediate (**L₀**) (c), and layer-like (**L**) (d) structures. The scheme of director distributions in the central cross-section (first row). Microphotographs in the unpolarized light (second row), at switched-off analyzer (third row), and in the crossed polarizers (fourth row). All microphotographs are of the same scale.